RESEARCH ARTICLE | JULY 15 2024

Toward a numerically efficient description of bulk-solvated anionic states

Matheus B. Kiataki ; Kaline Coutinho ; Márcio T. do N. Varella

J. Chem. Phys. 161, 034301 (2024)
https://doi.org/10.1063/5.0203247

The Journal of Chemical Physics ARTICLE pubs.aip.org/aip/jcp

Toward a numerically efficient description of bulk-solvated anionic states

Cite as: J. Chem. Phys. 161, 034301 (2024); doi: 10.1063/5.0203247
Submitted: 11 February 2024 • Accepted: 27 June 2024 •
Published Online: 15 July 2024

Matheus B. Kiataki,[a] Kaline Coutinho,[b] and Márcio T. do N. Varella[c]

AFFILIATIONS

Instituto de Física, Universidade de São Paulo, Rua do Matão 1731, 05508-090 São Paulo, Brazil

[a]Author to whom correspondence should be addressed: kiatakimatheus@gmail.com and kiataki@usp.br
[b]Electronic mail: kaline@if.usp.br
[c]Electronic mail: mvarella@if.usp.br

ABSTRACT

We investigate the vertical electron attachment energy (VAE) of 1-methyl-4-nitroimidazole, a model radiosensitizer, employing quantum mechanics/molecular mechanics (QM/MM) and QM/polarized continuum (QM/PCM) solvation models. We considered the solvent-excluded surface (QM/PCM-SES) and Van der Waals (QM/PCM-VDW) cavities within the PCM framework, the electrostatic embedding QM/MM (EE-QM/MM) model, and the self-consistent sequential QM/MM polarizable electrostatic embedding (scPEE-S-QM/MM) model. Due to slow VAE convergence concerning the number of QM solvent molecules, full QM calculations prove inefficient. Ensemble averages in these calculations do not align with VAEs computed for the representative solute–solvent configuration. QM/MM and QM/PCM calculations show agreement with each other for sufficiently large QM regions, although the QM/PCM-VDW model exhibits artifacts linked to the cavity. QM/MM models demonstrate good agreement between ensemble averages and VAEs calculated with the representative configuration. Notably, the VAE computed with the scPEE-S-QM/MM model achieves faster convergence concerning the number of QM water molecules compared to the EE-QM/MM model, attributed to enhanced efficiency from MM charge polarization in the scPEE-S-QM/MM approach. This emphasizes the importance of QM/classical models with accurate solute–solvent and solvent–solvent mutual polarization for obtaining converged VAEs at a reasonable computational cost. The full-QM approach is very inefficient, while the microsolvation model is inaccurate. Computational savings in QM/MM models result from electrostatic embedding and the representative configuration, with the scPEE-S-QM/MM approach emerging as an efficient tool for describing bulk-solvated anions within the QM/MM framework. Its potential extends to improving transient anion state descriptions in biomolecules and radiosensitizers, especially given the frequent employment of microsolvation models.

I. INTRODUCTION

Biological environments can be exposed to ionizing radiation originating from both natural and artificial sources.[1,2] The interaction between ionizing radiation and water molecules, proteins, and salts within biological media gives rise to a substantial production of secondary species, notably electrons and reactive species capable of attacking DNA. Among those secondary species, low-energy electrons, with kinetic energies below 30 eV, can be involved in a variety of DNA lesions, such as single- and double-strand breaks, base damage, crosslinks, and clustered lesions, which are particularly difficult to repair.[3–9] The origin of those lesions primarily stems from transient anion states, known as resonances, formed through electron capture events. The transient anions may decay through autoionization (electron detachment) or undergo dissociative electron attachment (DEA) reactions.

Although DNA lesions induced by the formation of resonances are unwelcome in healthy tissues, they could be beneficial when directed at tumor cells. Radiosensitizing drugs have been considered to increase the damage to the DNA of cancer cells in chemo-radiation cancer treatments.[6,7,10] Nitroimidazoles comprise an important class of electron-affinic radiosensitizers intended to treat radioresistant hypoxic tumors.[11] Experimental studies performed in the gas phase have shown that nitroimidazoles are susceptible to decomposing under exposure to low-energy electrons.[12–16] Most of these studies have advocated that radicals generated by the decay of resonances of nitroimidazoles via DEA may play an important role in their action as radiosensitizing drugs inside hypoxic

cells. However, recent experiments carried out for nitroimidazolic compounds[17,18] as well as for other molecules[19] in microhydrated environments have already shown that some DEA channels that were open in the gas phase were suppressed in the presence of a few water molecules. Thus, water molecules that are ubiquitous in biological media are expected to significantly affect the resonances and DEA processes of biomolecules and anticancer drugs.

Even though the aforementioned and other relevant studies[20–29] have partially considered solvent effects by including a microsolvation environment, it is still unclear how the bulk water environment would affect the formation of resonances and the subsequent processes. From a computational point of view, investigating the effects of bulk solvation on resonances is far from trivial. Unlike bound anion states (stable against autoionization), resonant states cannot be fully described by standard electronic structure methods. To describe the transient electronic states, one usually resorts to scattering[30] or modified electronic structure methods[31] that account for the autoionization probability. In view of the inherent difficulties in accounting for the autoionization probabilities, which pose challenges to the inclusion of solvation effects, most studies are restricted to the resonance spectra of biologically relevant molecules in the gas phase or microhydrated environments. Even bound anion states can pose challenges to computational models. Although those states can in principle be described with hybrid quantum mechanical (QM)/classical approaches,[32] electron attachment changes the charge of the solute, thus inducing polarization effects on the solvent molecules, which are not easily accounted for.[33–41]

The central idea of the hybrid QM/classical models consists of splitting the system into a part treated quantum mechanically (QM region), while the remaining part (classical region) is described by a classical model, such as molecular mechanics (MM) force fields[42,43] or polarizable continuum models (PCMs).[44,45] PCMs provide a straightforward way to incorporate the solvent, which is assumed to be a polarizable dielectric continuum. The solute is accommodated in a cavity with a suitably chosen shape carved into the dielectric medium. The QM charge density of the solute polarizes the dielectric medium, and it is also back polarized until the solute-dielectric system reaches equilibrium. The QM/PCM approach, therefore, takes into account the mutual polarization between the QM solute and the classical region (continuum medium). However, as the environment is assumed to be a continuum, those polarization effects are accounted for macroscopically, i.e., averaged over the solvent molecules. For instance, site-to-site interactions such as hydrogen bonding are typically poorly described by continuum models. One way to overcome this shortcoming is by expanding the QM partition, i.e., including some explicit solvent molecules into the QM region embedded in the continuum.

In turn, the QM/MM models keep the atomistic character of the solvent at the expense of requiring an explicit sampling of the configurational space of the solute–solvent system.[42,43] Different approaches are used to describe the interactions between the QM and MM regions, which usually involve bonding, van der Waals, and electrostatic terms. The electrostatic interaction, which is the most important one, can be treated with several levels of sophistication. The simplest approach, called mechanical embedding QM/MM, considers the electrostatic interaction at the MM level. Its main shortcoming is not accounting for the polarization of the QM wave function by the MM environment. The improved electrostatic embedding QM/MM (EE-QM/MM) model incorporates the field of the MM effective charges in the QM region. EE-QM/MM approaches are widely employed and even consider the systematic expansion of the QM region.[46–51] The strategy of including some QM solvent surrounding the solute partly recovers the mutual polarization among molecules, which is missed in the standard EE-QM/MM model that treats only the solute as QM. The main bottleneck of the systematic expansion of the QM region is obviously the scaling of the computational effort with the QM partition size.

Finally, the polarizable embedding schemes allow the MM atoms to be polarized by the QM region. One can mention the Drude oscillator model,[33,34] the fluctuation charge model,[35,36] the induced dipole moment model,[37,38] and the Self-Consistent Electrostatic Embedding (SCEE) model.[39,40] We recently proposed the self-consistent sequential QM/MM polarizable electrostatic embedding (scPEE-S-QM/MM)[41] model to account for the fast solute–solvent and solvent–solvent mutual polarization effects within the EE framework. The method is based on the sequential QM/MM (S-QM/MM) approach, where solute–solvent configurations are first generated with MC simulations, while quantum calculations are performed subsequently on statistically uncorrelated configurations to obtain averaged electronic properties of interest.[52] The core concept of the scPEE-S-QM/MM methodology is dividing the solute–solvent configurations into smaller parts, typically individual molecules, which are treated as QM subsystems subjected to the EE field generated by all the remaining molecules. Atomic charges for each individual molecule are recalculated from the QM computations employing the CHELPG[53] method, and the procedure is repeated iteratively until all atomic charges and dipole moments are converged. From the individual charges and dipole moments, one can understand, e.g., how different electronic states of neutral and anionic solutes polarize their environment or assess the impact of the solvent polarization on the electronic properties of the solute. The scPEE-S-QM/MM method provides accurate results for the dipole moment of liquid water as well as for the gas-to-liquid change in the dipole moment of water molecules.[41]

In the present study, we delved into understanding how both micro and bulk solvation affect the bound anion state of 1-methyl-4-nitroimidazole (1M4NI). This molecule is a well-known radiosensitizer model that has been extensively studied in the gas phase, particularly under low-energy electron exposure. Its structural similarities to nimorazole, a recognized radiosensitizer employed in some cancer treatments,[18] render it an intriguing system for investigation, principally under the influence of water molecules. As mentioned, a substantial research gap exists in understanding the effects of bulk solvation on anion states, especially in simulating intricate transient anions, where studies have predominantly focused on microsolvation effects. Given the stability of bound anion states against autoionization, we can leverage standard electronic structure methods along with diverse available hybrid QM/classical solvation models to understand the influence of bulk water on these states and, by extension, indirectly on resonant states. Here, we focus on comprehending how bulk solvation modeled by different hybrid QM/classical models affects the π_1^* valence bound anion state of 1M4NI. Emphasis is placed on the vertical electron attachment energy ($VAE_{\pi_1^*}$) property, also referred to as the negative of vertical electron affinity (−VEA), and on the EE polarization resulting

from the vertical electron attachment process. Moreover, we shed light on (i) the marked distinctions between the effects of micro and bulk solvation on VAE; (ii) the crucial role played by the classical region enclosing the QM region; (iii) the paramount significance of accounting for the rapid solute–solvent and solvent–solvent mutual polarization effects when describing bulk-solvated anions; (iv) the limitations, strengths, and reliability of the well-known solvation models explored here; and (v) the individual impact of each water molecule within bulk water on VAE.

II. METHODS

The present work is based on the sequential QM/classical approach.[52] While the classical step consists of Monte Carlo (MC) simulations using force fields and rigid molecular geometries, different strategies are considered in the subsequent QM step. The latter calculations are performed for a set of statistically uncorrelated solute–solvent configurations employing QM methods for the whole system (full-QM), as well as QM/PCM, EE-QM/MM, and scPEE-S-QM/MM models. In all cases, the convergence of the calculated VAEs was investigated by systematically increasing the number of QM water molecules.

A. Monte Carlo simulations

The QM single-point calculations were performed employing solute–solvent configurations generated via MC simulations, as described in our previous study.[41] The MC simulations were performed with the DICE software[54] in the *NPT* ensemble (298.15 K and 1 atm) using standard numerical procedures. Solute–solvent configurations consisting of a single 1M4NI neutral molecule surrounded by 1000 water molecules were generated from those simulations. The solute and solvent molecules were considered rigid during the MC simulations, such that only the rotation–translation configuration state was sampled. The ground state geometry of 1M4NI was optimized with the density functional theory (DFT), employing the B3LYP exchange–correlation functional[55,56] and the aug-cc-pVDZ basis set, as implemented in Gaussian 09.[57] We employed the gas-phase optimal geometry in the MC simulations since no significant differences were found with respect to the optimal geometry obtained in an aqueous PCM environment.[58]

The MM charges of the solute were obtained from the CHELPG procedure,[53] where the electronic density was generated with second-order Møller–Plesset perturbation theory (MP2) and the aug-cc-pVDZ basis set. In these calculations, the solute was surrounded by a PCM aqueous medium, such that solute polarization effects were incorporated into the MM charges.[59,60] The interatomic interactions were described with conventional Coulomb and Lennard-Jones (LJ) potentials. The all-atom optimized potentials for liquid simulations (OPLS-AA) parameters[61] were used for the solute, while the extended simple point charge[62] (SPC/E) parameterization and molecular geometries were employed for water.

B. Single-point calculations

A subset of statistically uncorrelated solute–solvent configurations obtained from the analysis of the autocorrelation function of the energy,[52] containing 500 solvent molecules, was selected to perform the subsequent single-point calculations for the full-QM and QM/classical models. Those configurations are separated by 8000 MC cycles (decorrelation range), where each cycle involves the movement of all the molecules in the simulation box (rotation–translation configuration space, employing rigid molecular geometries). In each configuration, three water molecules form hydrogen bonds (HBs) with the solute, corresponding to the average number of HBs in the microsolvation shell.[41]

The VAE of the π_1^* anion ground state, denoted as $VAE_{\pi_1^*}$, was computed as the energy difference between the ground electronic states of the anion and the neutral forms, computed at the B3LYP/6-31+G(d) level, in the optimized geometry of the neutral species (VAE_{π^*} thus corresponds to the negative of vertical electron affinity, −VEA). The calculations were performed for the representative configuration defined in our previous study, which has HB properties and solute orbital energies close to the ensemble averaged values.[41] We also considered several solvent models, namely, full-QM, QM/PCM, EE-QM/MM, and scPEE-S-QM/MM. We emphasize that the full-QM model treats the solute and solvent molecules quantum mechanically, where the latter species are referred to as QM water molecules.

The QM/PCM calculations explored the Solvent Excluded Surface (SES) and Van der Waals (VDW) cavity models using the default parameters implemented in Gaussian09.[57] Since we are interested in the solvent polarization response to vertical electron attachment, we considered the ground-state geometry of the neutral molecule. Using this geometry, non-equilibrium PCM calculations were performed for the neutral and anion species, while the VAEs were obtained as energy differences.

In the EE-QM/MM model, the electrostatic embedding environment is described with SPC/E static point charges. We investigated the convergence of $VAE_{\pi_1^*}$ against the number of molecules in the QM regions for all solvent models. In addition, averages of over 40 statistically uncorrelated configurations were performed for all the explicit solvation models. These averages were restricted to modest sized QM regions due to the scaling of the numerical effort.

The scPEE-S-QM/MM calculations follow the protocol described previously.[41] Each of the 40 configurations is divided into two parts, namely, (i) a cluster composed of the 1M4NI solute and the three water molecules forming HBs, and (ii) the remaining 500 water molecules. The cluster, either in neutral or anionic form, was initially polarized in the PCM environment at the B3LYP/6-31+G(d) level, so MM charges could be generated with the CHELPG[53] method. The remaining water molecules were then individually polarized by treating each one of them quantum mechanically, subjected to the field generated by the EE consisting of all other solvent and solute molecules. The MM charges and dipole moment were recalculated for the individual QM water molecules with the CHELPG method at MP2/6-31G(d). While, in principle, the procedure should be repeated until all the effective charges of the solute and the dipole moment of the solvent molecules are converged, in practice we found that a single polarization cycle for the solvent molecules was sufficient.

$VAE_{\pi_1^*}$ estimates for the largest quantum region, containing 240 QM water molecules, were also obtained with the scPEE-S-QM/MM model using different DFT functionals and the 6-311+G(d,p) basis set, namely, B3LYP, CAM-B3LYP,[63] M06-2X,[64] ωB97X,[65] and ωB97XD.[66]

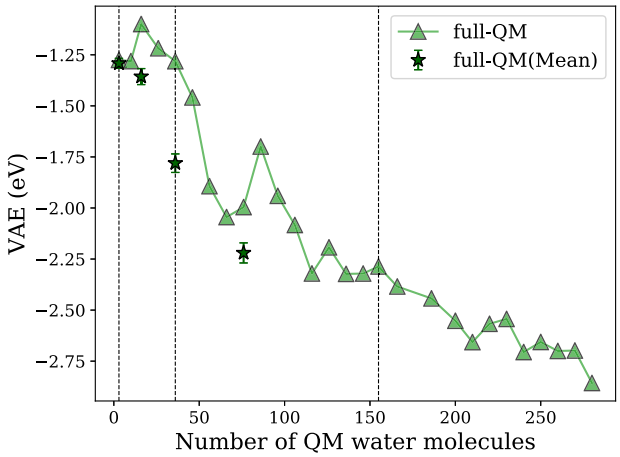

FIG. 1. $VAE_{\pi_1^*}$ obtained from full-QM calculations with the B3LYP/6-31+G(d) method as a function of the number of water molecules in the QM region. The triangles indicate the results obtained for the representative configuration, while the stars indicate the mean values (averages over uncorrelated configurations). The vertical lines indicate the microsolvation shell (3 water molecules), the first solvation shell (36 accumulated water molecules), and the second solvation shell (155 accumulated water molecules). Error bars represent the standard errors.

III. RESULTS AND DISCUSSIONS

The $VAE_{\pi_1^*}$ estimates obtained with the full-QM model for the representative configuration are shown in Fig. 1 (triangles). The results were obtained by increasing the number of quantum water molecules from zero (the isolated 1M4NI solute) to 280. Solvent molecules are included from the nearest to farthest in accordance with the minimum distance distribution function. As discussed elsewhere,[41] there are 36 and 155 water molecules up to the end of the first and second solvation shells, respectively, so the full-QM clusters with 280 solvent molecules can be considered large. We also show $VAE_{\pi_1^*}$ results obtained by averaging over 40 configurations (stars). For the smaller full-QM models, containing up to 3 solvent molecules, there is good agreement between the mean values and those computed for the representative configuration. This behavior can be understood since three water molecules form HBs (microsolvation shells) in the 40 uncorrelated configurations considered in the average and also in the representative one (see Sec. II B). Despite the discrepancies observed for larger full-QM clusters, the slow convergence of the VAE with respect to the number of solvent molecules is remarkable in both cases. The $VAE_{\pi_1^*}$ values have a significant slope beyond the first solvation shell, while a similar behavior persists even beyond the second solvation shell for the representative configuration. The $VAE_{\pi_1^*}$ estimates under microsolvation (three water molecules) are −1.28 and −1.29(2) eV for the representative configuration and the average of the uncorrelated configurations, respectively, such that the VAE is reduced by ≈1 eV compared to the gas phase. The stabilization occurs because the solvent molecules act as donors in the HBs formed with the solvent. The full-QM results were also computed with the CAM-B3LYP functional and the 6-31+G(d) basis set, considering the representative configuration and clusters with up to 250 QM solvent molecules. The comparison between the B3LYP and CAM-B3LYP results is shown in Fig. 2. The VAE converges slowly, with significant oscillations for both functionals. However, significant discrepancies between the VAEs obtained with CAM-B3LYP and B3LYP

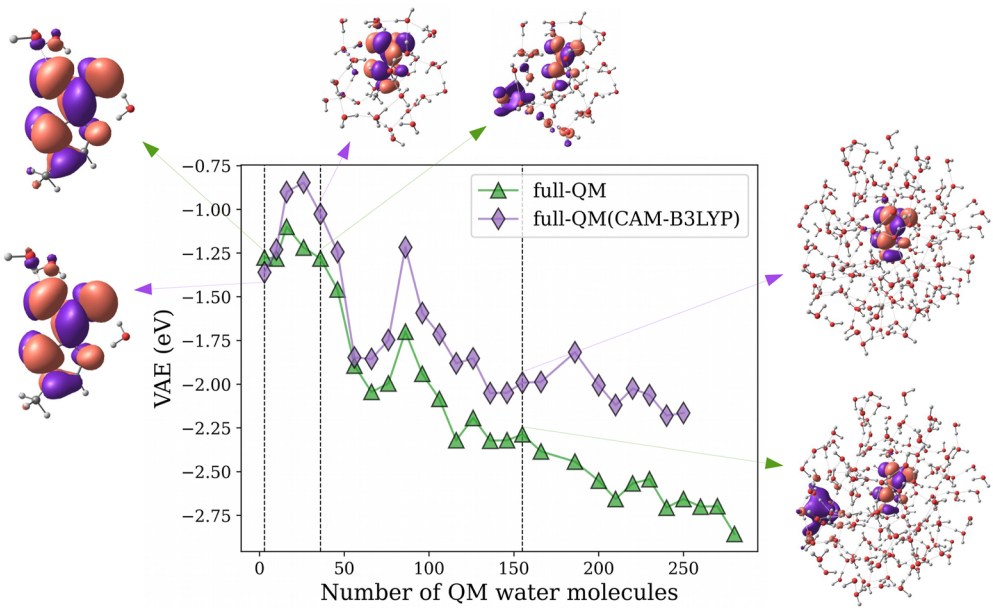

FIG. 2. Comparison between the VAE obtained from full-QM calculations with the CAM-B3LYP/6-31+G(d) functional (purple diamonds) and the B3LYP/6-31+G(d) functional (green triangles in Fig. 1) as a function of the number of water molecules in the QM region. Both curves were computed for the representative configuration. The vertical lines indicate the microsolvation shell (3 water molecules), the first solvation shell (36 accumulated water molecules), and the second solvation shell (155 accumulated water molecules). SOMO figures are shown for each solvation shell.

also exist, and they tend to increase with cluster size. The anion stabilization in the B3LYP calculations is related to the partial delocalization of the excess charge density over the solvent molecules, as indicated by the singly occupied molecular orbital (SOMO) plots in Fig. 2. In contrast, the CAM-B3LYP functional predicts excess charges localized around the solute molecule. Our results are consistent with previous studies on charge-transfer contamination in the condensed phase[67,68] and the vanishing HOMO–LUMO gap in proteins and water clusters.[69,70] The unphysical charge delocalization was attributed to the inaccurate treatment of the long-range Coulomb interaction in hybrid functionals (without exact Hartree–Fock exchange in the outer region), edge water molecules in the cluster–vacuum boundary, and electrostatic effects arising from the very large dipole moments of the QM aggregates. Nevertheless, it was also pointed out that the inclusion of an electrostatic embedding (EE-QM/MM model) mitigates the problem.[68–70] In fact, the VAEs calculated with the B3LYP and CAM-B3LYP functionals show essentially the same behavior in the presence of the SPC/E and polarized embeddings (see Figs. S1 and S2). The SOMO remains localized around the solute, and the discrepancy between the VAEs is fairly constant over a broad range of system sizes (B3LYP predicts slightly less stable anions, approximately by 0.1 eV). Since our main concern is the polarization of the EE, the most relevant aspects of Figs. 1 and 2 are the slow convergence of the full-QM model with respect to the cluster size, even for the range-separated CAM-B3LYP functional, and the disagreement between the mean VAEs and those computed for the representative configuration.

Since the full-QM calculations converge slowly, we consider several QM/classical approaches as alternatives. Figure 3 shows $VAE_{\pi_1^*}$ results in bulk water computed with the EE-QM/MM,

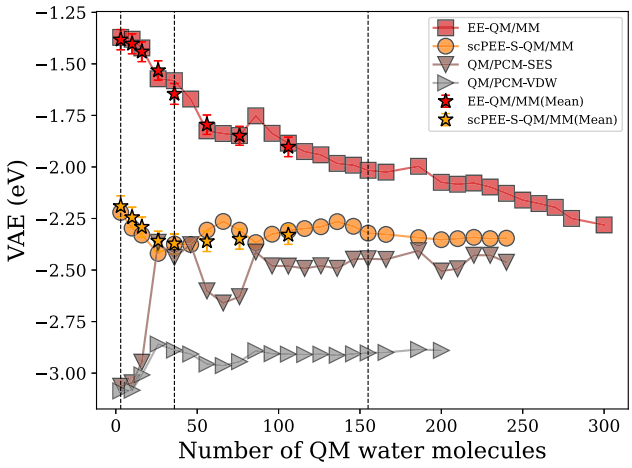

FIG. 3. $VAE_{\pi_1^*}$ obtained from different QM/classical models with the B3LYP/6-31+G(d) method, as a function of the number of water molecules in the QM region. Squares (EE-QM/MM), circles (scPEE-S-QM/MM), brown triangles (QM/PCM-SES), and gray triangles (QM/PCM-VDW) indicate the results obtained for the representative configuration, while the stars indicate the mean values (averages over uncorrelated configurations) for each solvation model. Vertical lines indicate the microsolvation shell (3 water molecules), the first solvation shell (36 water molecules), and the second solvation shell (155 water molecules). Error bars represent the standard errors.

TABLE I. $VAE_{\pi_1^*}$ (in eV) obtained for the representative configuration using various solvation models and QM regions with different numbers of water molecules. The mean values, $\langle VAE_{\pi_1^*} \rangle$, and standard errors (the latter in parenthesis) are indicated.

Model	QM	MM	$VAE_{\pi_1^*}$	$\langle VAE_{\pi_1^*} \rangle$
Gas	0	0	− 0.32	
Full-QM	3	0	−1.28	−1.29(2)
	36	0	−1.28	−1.78(5)
	106	0	−2.08	···
	155	0	−2.29	···
	240	0	−2.71	···
EE-QM/MM	3	500	−1.37	−1.38(5)
	36	467	−1.58	−1.65(5)
	106	397	−1.88	−1.90(5)
	155	348	−2.02	···
	240	263	−2.13	···
scPEE-S-QM/MM	3	500	−2.22	−2.19(5)
	36	467	−2.37	−2.37(5)
	106	397	−2.31	−2.33(5)
	155	348	−2.32	···
	240	263	−2.35	···
QM/PCM-SES	3	0	−3.06	···
	36	0	−2.44	···
	106	0	−2.48	···
	155	0	−2.45	···
	240	0	−2.46	···
QM/PCM-VDW	3	0	−3.09	···
	36	0	−2.89	···
	106	0	−2.91	···
	155	0	−2.90	···
	240	0	···	···

QM/PCM-VDW, QM/PCM-SES, and scPEE-S-QM/MM models. Once more, we analyzed the representative configuration and averaged over 40 uncorrelated configurations, only for QM partitions containing up to 106 water molecules in the latter case. The results obtained with the various classical models for the water environment are generally not in good agreement, especially for the calculations with fewer QM water molecules. Nevertheless, compared to the full-QM model (Fig. 1), the QM/classical results show smoother oscillations and smaller slopes, i.e., they converge faster. Furthermore, the charge delocalization problem for the B3LYP functional is mitigated, as discussed above. More importantly, there is always good agreement between the $VAE_{\pi_1^*}$ estimates obtained for the representative configuration and the averaged values, which allows for significant savings in computational time. Among the classical models, EE-QM/MM, which neglects solvent polarization, has the slowest convergence. The results indicate that the inclusion of the solvent environment is essential since EE-QM/MM is clearly superior to full-QM, but solvent polarization is also crucial to obtain converged energies with a reasonably small number of QM water molecules, as discussed further on. Apart from QM/PCM-VDW, the QM/classical models predict $VAE_{\pi_1^*} \approx -2.3$ eV for large enough QM regions (see also Table I). It should be remembered that QM/PCM-SES, which

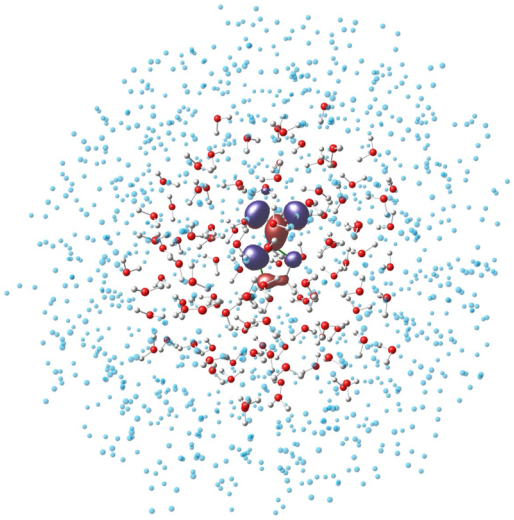

FIG. 4. Singly occupied molecular orbital (SOMO) of the 1M4NI anion having π_1^* character. The calculation was performed with the B3LYP/6-31+G(d) method within the scPEE-S-QM/MM framework, considering the representative configuration of 106 QM water molecules and 397 MM molecules (polarized atomic charges).

is consistent with the QM/MM models, describes the classical environment as a dielectric continuum. The disagreement between the continuum models (QM/PCM-SES and QM/PCM-VDW), despite their fast convergence, could arise from voids in the VDW cavity.[71]

The size of the QM region slightly affects the $VAE_{\pi_1^*}$ calculated with the scPEE-S-QM/MM model. The results only fluctuate within a narrow range (−2.22 to −2.35 eV) as the number of QM solvent molecules increases from 3 to 240, which indicates that much of the mutual solute–solvent and solvent–solvent polarization is accounted for by the polarized atomic charges. Although the fluctuations decrease in magnitude until 155 water molecules are included in the QM partition, reasonably accurate results could be obtained using only the QM microsolvation shell. Thus, larger QM regions are effectively replaced by the properly polarized MM environment. It is worth emphasizing the good agreement between the $VAE_{\pi_1^*}$ estimates obtained with the scPEE-S-QM/MM model for the representative configuration and the average values. Our most robust result in bulk water, $VAE_{\pi_1^*} = -2.35$ eV, was obtained with the scPEE-S-QM/MM method for the representative configuration considering 240 QM water molecules and 263 MM water molecules described with polarized atomic charges (see Table I). Our best estimate for the ensemble average, $\langle VAE_{\pi_1^*} \rangle = -2.33(5)$ eV was also computed with the scPEE-S-QM/MM method, although considering 106 QM and 397 MM water molecules (polarized atomic charges). Bulk solvation, as described by scPEE-S-QM/MM, stabilizes the $VAE_{\pi_1^*}$ by ≈2 eV compared to the gas phase, significantly differing from the stabilization induced by full-QM microsolvation (≈1 eV). The PCM models overestimate the stabilization of the VAE in the bulk limit (QM 1M4NI solute plus PCM environment), compared to our best results, since QM/PCM-SES and QM/PCM-VDW provide, respectively, $VAE_{\pi_1^*} = -2.93$ eV and $VAE_{\pi_1^*} = -2.83$ eV.

The comparison between the scPEE-S-QM/MM and EE-QM/MM models also corroborates the improvement brought by the polarized electrostatic embedding. The latter model, which neglects mutual polarization, exhibits a notably slow convergence compared to the scPEE-S-QM/MM model. scPEE-S-QM/MM provides the most efficient description of bulk solvation on the $VAE_{\pi_1^*}$ of 1M4NI,

TABLE II. $VAE_{\pi_1^*}$ (in eV) for the 1M4NI molecule in bulk water computed with the scPEE-S-QM/MM model and the 6-311+G(d,p) basis set using different exchange–correlation functionals. The calculations considered 240 QM water molecules and 263 MM water molecules (polarized point charges).

	B3LYP	CAM-B3LYP	M06-2X	ωB97X	ωB97XD
$VAE_{\pi_1^*}$	−2.38	−2.44	−2.42	−2.38	−2.29

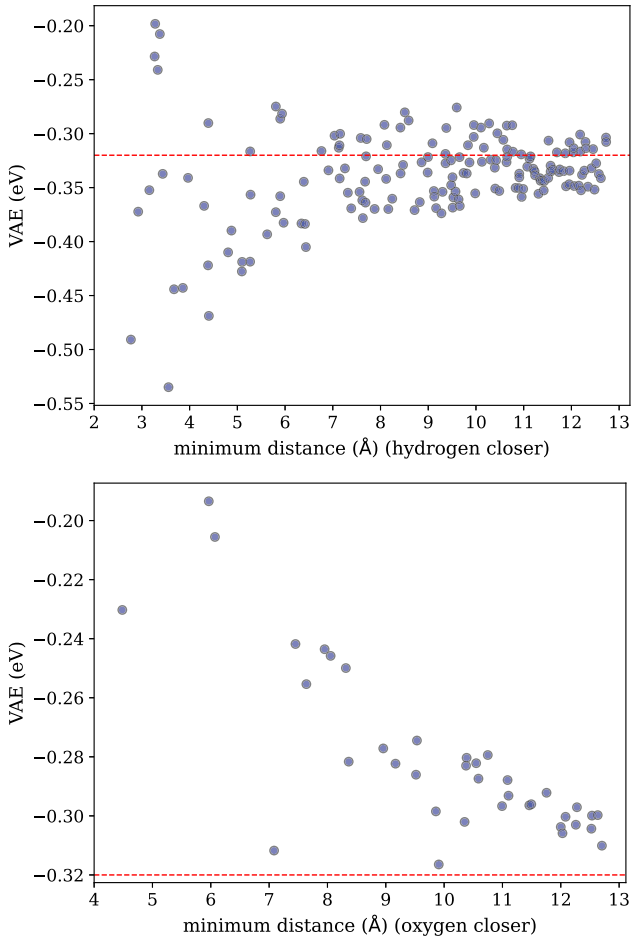

FIG. 5. $VAE_{\pi_1^*}$ for 1M4NI–H_2O pairs as a function of the minimum distance between the atoms of the solvent molecules and the atoms belonging to the ring and nitro group of the solute. Top panel: water molecules with one hydrogen atom closer to the solute. Bottom panel: water molecules with the oxygen atom closer to the solute. Horizontal lines indicate the VAE in the gas phase.

among the models investigated in this study. A depiction of the additional electron attached to the 1M4NI in polarized bulk water is shown in Fig. 4.

Although EE polarization is our main interest, for completeness, we calculated the $VAE_{\pi_1^*}$ with other DFT functionals and the 6-311+G(d,p) basis set within the scPEE-S-QM/MM framework. The calculations were carried out for the representative configuration, considering 240 QM water molecules and 263 MM water molecules (polarized point charges). As shown in Table II, the results are consistent with the previous B3LYP/6-31+G(d) estimate (−2.35 eV). The B3LYP calculations performed with the 6-31+G(d) and 6-311+G(d,p) basis sets agree within 0.03 eV. The ωB97XD functional provided the most discrepant result, with deviations around 0.09–0.15 eV compared to the other functionals.

Again using the representative configuration, we examined the individual contributions of solvent molecules to the $VAE_{\pi_1^*}$ by considering 1M4NI–H_2O pairs. We performed QM calculations for the pairs, selecting individual solvent molecules according to the following procedure: We used the minimum distance distribution function to identify the water molecules that are closer to atoms belonging to the ring or nitro group of the 1M4NI molecule (the excess charge of the solute is mostly located on this group of atoms; see Fig. 4. Among the selected solvent molecules, we further identified those in which hydrogen or oxygen atoms are closer to the solute. The $VAE_{\pi_1^*}$ for the 1M4NI–H_2O pairs are shown in Fig. 5 as a function of the minimum distance. The results for the solvent molecules with hydrogen and oxygen atoms lying closer to the solute are shown in the top and bottom panels, respectively. When one hydrogen atom is closer to the solute (top panel), the $VAE_{\pi_1^*}$ can be either stabilized or destabilized compared to the gas phase. As shown in the top panel in Fig. 6, the $VAE_{\pi_1^*}$ is destabilized when water molecules have hydrogen atoms oriented away from the ring and nitro group, while stabilized when the hydrogen atoms are oriented toward those atoms (see the bottom panel in Fig. 6). On the

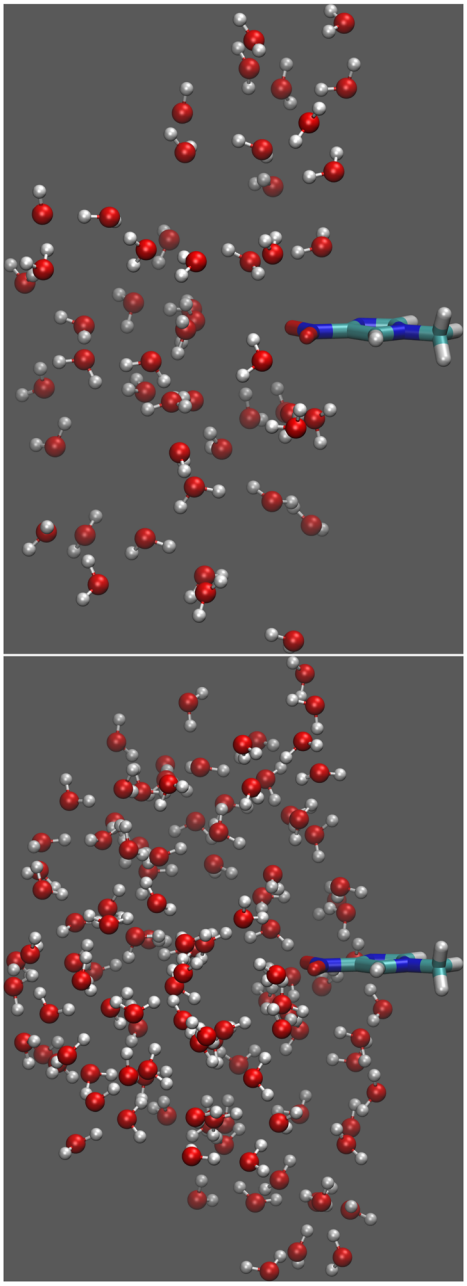

FIG. 6. Superposition of the 1M4NI–H_2O pairs in which a hydrogen atom of the solvent molecule is closer to the solute (corresponding to the top panel in Fig. 5). Top panel: pairs with $VAE_{\pi_1^*}$ destabilized with respect to the gas phase. Bottom panel: pairs with $VAE_{\pi_1^*}$ stabilized with respect to the gas phase.

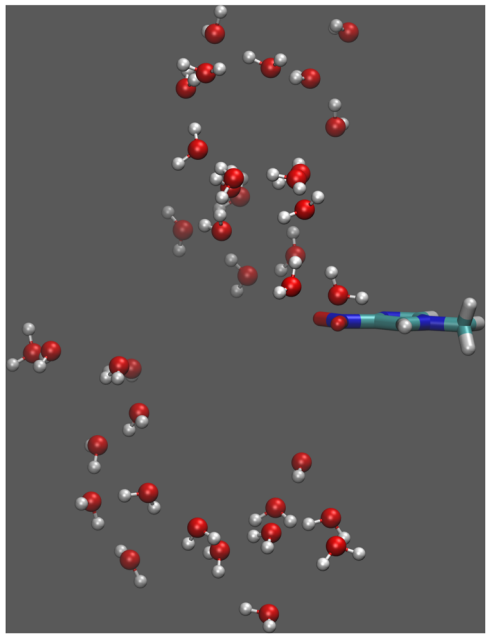

FIG. 7. Superposition of the 1M4NI–H_2O pairs in which the oxygen atom of the solvent molecule is closer to the solute (corresponding to the bottom panel in Fig. 5). In all pairs, the $VAE_{\pi_1^*}$ was destabilized with respect to the gas-phase.

other hand, when the oxygen atoms are closer to the ring or nitro group, the $VAE_{\pi_1^*}$ is always destabilized (see the bottom panel in Figs. 5 and 7).

While interactions between pairs can be screened by other solvent molecules in the liquid, there is a clear indication that the VAE tends to be stabilized when the positively charged hydrogen atoms of the solvent are oriented toward the negatively charged groups of the solute. This finding supports previous studies of microsolvated resonances, which identified that anion states are stabilized when water molecules act as donors in hydrogen bonds.[20,22–24,27] Nonetheless, the previous discussion indicates that microsolvation models may not accurately describe the features of bulk-solvated anion states. Although the current understanding of solvated resonances in small biomolecules and radiosensitizing drugs is largely based on microsolvation,[17–25,27,28] our results indicate that computational models should seek the bulk solvation limit. To achieve this goal, the scPEE-S-QM/MM model can efficiently produce VAE estimates that are reasonably converged without the need for large QM regions.

IV. CONCLUSIONS

We examined the $VAE_{\pi_1^*}$ of the 1M4NI molecule using both standard QM/classical solvation models and the recently introduced scPEE-S-QM/MM model. In general, the full-QM calculations were inefficient in view of the high computational cost, slow convergence, and the need to perform ensemble averages. The additional charge spuriously delocalized over the solvent molecules when the B3LYP functional was used. In the full-QM calculations performed with the CAM-B3LYP functional, the charge remained localized around the solute, and the convergence was clearly improved with respect to B3LYP, although still rather slow.

The QM/MM and QM/PCM calculations agree with each other for large enough QM regions, although the QM/PCM-VDW model seems to be plagued by artifacts related to the cavity. The convergence of the EE-QM/MM calculations with respect to the size of the QM region is rather slow, requiring at least 300 QM water molecules, although the EE mitigates the charge delocalization problem for the B3LYP functional. While scPEE-S-QM/MM and QM/PCM-SES are rapidly converging, the former model is more efficient since the $VAE_{\pi_1^*}$ shows smaller fluctuations even for moderately sized QM regions. The results point out that QM/classical models with a proper description of solute–solvent and solvent–solvent mutual polarization are essential to obtain converged VAE values at a reasonable computational cost. The full-QM approach is very inefficient, while the microsolvation model is inaccurate. The computational savings of QM/MM models over full-QM calculations are due to both the electrostatic embedding, thus replacing QM molecules, and the ability to use only the representative configuration, thus eliminating the ensemble averages.

We also investigated the $VAE_{\pi_1^*}$ of 1M4NI-water pairs as a function of the minimum distance to the atoms in the ring and nitro group of the solute. Independent of the distance, the VAE tends to be stabilized by solvent molecules with a hydrogen atom oriented toward the ring and nitro group and destabilized for other orientations (especially oxygen atoms oriented toward the solute). The latter outcome aligns with earlier research on microsolvated resonances, which indicates that hydrogen bonds where water molecules act as donors tend to stabilize the transient anion states. However, improved models for solvated anionic states of biomolecules and radiosensitizing drugs must go beyond microsolvation. The scPEE-S-QM/MM technique seems to be an efficient numerical tool to describe bulk-solvated anions within the QM/MM framework.

SUPPLEMENTARY MATERIAL

The supplementary material contains additional VAE results and SOMO figures.

ACKNOWLEDGMENTS

M.B.K. acknowledges the financial support from FAPESP (Grant No. 2023/07835-2) and CNPq (Grant No. 142103/2019-5). M.T. do N.V. also acknowledges the financial support from (CNPq) (Grant No. 306285/2022-3) and FAPESP (Grant No. 2020/16155-7). K.C. acknowledges the financial support from FAPESP (Grant No. 2021/09016-3). K.C. and M.B.K. also acknowledge the National Institute of Science and Technology Complex Fluids (INCT-FCx), financed by CNPq (Grant No. 141260/2017-3) and FAPESP (Grant No. 2014/50983-3). The calculations were partly performed with HPC resources from STI, University of São Paulo.

AUTHOR DECLARATIONS

Conflict of Interest

The authors have no conflicts to disclose.

Author Contributions

Matheus B. Kiataki: Conceptualization (equal); Data curation (equal); Formal analysis (equal); Investigation (equal); Methodology (equal); Project administration (equal); Software (equal); Supervision (equal); Validation (equal); Visualization (equal); Writing – original draft (equal); Writing – review & editing (equal). **Kaline Coutinho**: Conceptualization (equal); Formal analysis (equal); Funding acquisition (equal); Investigation (equal); Methodology (equal); Project administration (equal); Resources (equal); Software (equal); Supervision (equal); Writing – review & editing (equal). **Márcio T. do N. Varella**: Conceptualization (equal); Formal analysis (equal); Funding acquisition (equal); Investigation (equal); Methodology (equal); Project administration (equal); Resources (equal); Software (equal); Supervision (equal); Validation (equal); Visualization (equal); Writing – original draft (equal); Writing – review & editing (equal).

DATA AVAILABILITY

The data that support the findings of this study are available from the corresponding author upon reasonable request.

REFERENCES

[1]IAEA: Radiation in everyday life https://www.iaea.org/Publications/Factsheets/English/radlife, Accessed: 04 May 2022.

[2]J. Kohanoff, M. McAllister, G. A. Tribello, and B. Gu, "Interactions between low energy electrons and DNA: A perspective from first-principles simulations," J. Phys.: Condens. Matter **29**, 383001 (2017).
[3]B. Boudaïffa, P. Cloutier, D. Hunting, M. A. Huels, and L. Sanche, "Resonant formation of DNA strand breaks by low-energy (3 to 20 eV) electrons," Science **287**, 1658–1660 (2000).
[4]F. Martin, P. D. Burrow, Z. Cai, P. Cloutier, D. Hunting, and L. Sanche, "DNA strand breaks induced by 0–4 eV electrons: The role of shape resonances," Phys. Rev. Lett. **93**, 068101 (2004).
[5]E. Alizadeh and L. Sanche, "Precursors of solvated electrons in radiobiological physics and chemistry," Chem. Rev. **112**, 5578–5602 (2012).
[6]E. Alizadeh, T. M. Orlando, and L. Sanche, "Biomolecular damage induced by ionizing radiation: The direct and indirect effects of low-energy electrons on DNA," Annu. Rev. Phys. Chem. **66**, 379–398 (2015).
[7]M. Rezaee, R. P. Hill, and D. A. Jaffray, "The exploitation of low-energy electrons in cancer treatment," Radiat. Res. **188**, 123–143 (2017).
[8]Y. Shao, Y. Dong, D. Hunting, Y. Zheng, and L. Sanche, "Unified mechanism for the generation of isolated and clustered DNA damages by a single low energy (5–10 eV) electron," J. Phys. Chem. C **121**, 2466–2472 (2017).
[9]Y. Dong, Y. Gao, W. Liu, T. Gao, Y. Zheng, and L. Sanche, "Clustered DNA damage induced by 2–20 eV electrons and transient anions: General mechanism and correlation to cell death," J. Phys. Chem. Lett. **10**, 2985–2990 (2019).
[10]R. Schürmann, S. Vogel, K. Ebel, and I. Bald, "The physico-chemical basis of DNA radiosensitization: Implications for cancer radiation therapy," Chem. - Eur. J. **24**, 10271–10279 (2018).
[11]P. Wardman, "Chemical radiosensitizers for use in radiotherapy," Clin. Oncol. **19**, 397–417 (2007), part of Special Issue: Importance of Radiobiology to Cancer Therapy: Current Practice and Future Perspectives.
[12]K. Tanzer, L. Feketeová, B. Puschnigg, P. Scheier, E. Illenberger, and S. Denifl, "Reactions in nitroimidazole triggered by low-energy (0–2 eV) electrons: Methylation at N1-H completely blocks reactivity," Angew. Chem., Int. Ed. **53**, 12240–12243 (2014).
[13]K. Tanzer, L. Feketeová, B. Puschnigg, P. Scheier, E. Illenberger, and S. Denifl, "Reactions in nitroimidazole and methylnitroimidazole triggered by low-energy (0–8 eV) electrons," J. Phys. Chem. A **119**, 6668–6675 (2015).
[14]A. Ribar, K. Fink, M. Probst, S. E. Huber, L. Feketeová, and S. Denifl, "Isomer selectivity in low-energy electron attachment to nitroimidazoles," Chem. - Eur. J. **23**, 12892–12899 (2017).
[15]R. Meißner, L. Feketeová, E. Illenberger, and S. Denifl, "Reactions in the radiosensitizer misonidazole induced by low-energy (0–10 eV) electrons," Int. J. Mol. Sci. **20**, 3496 (2019).
[16]R. Meißner, L. Feketeová, A. Bayer, P. Limão-Vieira, and S. Denifl, "Formation of negative and positive ions in the radiosensitizer nimorazole upon low-energy electron collisions," J. Chem. Phys. **154**, 074306 (2021).
[17]M. Ončák, R. Meißner, E. Arthur-Baidoo, S. Denifl, T. F. M. Luxford, A. Pysanenko, M. Fárník, J. Pinkas, and J. Kočišek, "Ring formation and hydration effects in electron attachment to misonidazole," Int. J. Mol. Sci. **20**, 4383 (2019).
[18]R. Meißner, J. Kočišek, L. Feketeová, J. Fedor, M. Fárník, P. Limão-Vieira, E. Illenberger, and S. Denifl, "Low-energy electrons transform the nimorazole molecule into a radiosensitiser," Nat. Commun. **10**, 2388 (2019).
[19]J. Kočišek, A. Pysanenko, M. Fárník, and J. Fedor, "Microhydration prevents fragmentation of uracil and thymine by low-energy electrons," J. Phys. Chem. Lett. **7**, 3401–3405 (2016).
[20]T. C. Freitas, M. A. P. Lima, S. Canuto, and M. H. F. Bettega, "Electron collisions with the CH_2O–H_2O complex," Phys. Rev. A **80**, 062710 (2009).
[21]T. C. Freitas, K. Coutinho, M. T. do N. Varella, M. A. P. Lima, S. Canuto, and M. H. F. Bettega, "Electron collisions with the HCOOH· · ·(H_2O)n complexes (n = 1, 2) in liquid phase: The influence of microsolvation on the π^* resonance of formic acid," J. Chem. Phys. **138**, 174307 (2013).
[22]E. M. de Oliveira, T. C. Freitas, K. Coutinho, M. T. do N. Varella, S. Canuto, M. A. P. Lima, and M. H. F. Bettega, "Communication: Transient anion states of phenol. . .$(H_2O)n$ (n = 1, 2) complexes: Search for microsolvation signatures," J. Chem. Phys. **141**, 051105 (2014).
[23]A. Sieradzka and J. D. Gorfinkiel, "Theoretical study of resonance formation in microhydrated molecules. I. Pyridine-$(H_2O)_n$, n = 1, 2, 3, 5," J. Chem. Phys. **147**, 034302 (2017).
[24]A. Sieradzka and J. D. Gorfinkiel, "Theoretical study of resonance formation in microhydrated molecules. II. Thymine-$(H_2O)_n$, n = 1, 2, 3, 5," J. Chem. Phys. **147**, 034303 (2017).
[25]I. I. Fabrikant, "Electron attachment to molecules in a cluster environment: Suppression and enhancement effects," Eur. Phys. J. D **72**, 96 (2018).
[26]M. McAllister, N. Kazemigazestane, L. T. Henry, B. Gu, I. Fabrikant, G. A. Tribello, and J. Kohanoff, "Solvation effects on dissociative electron attachment to thymine," J. Phys. Chem. B **123**, 1537–1544 (2019).
[27]L. M. Cornetta, K. Coutinho, and M. T. do N. Varella, "Solvent effects on the π^* shape resonances of uracil," J. Chem. Phys. **152**, 084301 (2020).
[28]J. D. Gorfinkiel, "Electron collisions with molecules and molecular clusters," Eur. Phys. J. D **74**, 51 (2020).
[29]H. Abdoul-Carime, G. Thiam, F. Rabilloud, F. Charlieux, and J. Kopyra, "Chemistry in acetonitrile–water films induced by slow (<15 eV) electrons: Application to the earth and space chemistry," ACS Earth Space Chem. **6**, 1126–1132 (2022).
[30]F. A. Gianturco, D. G. Thompson, and A. Jain, "Electron-scattering from polyatomic molecules using a single-center-expansion formulation," in *Computational Methods for Electron—Molecule Collisions*, edited by W. M. Huo and F. A. Gianturco (Springer US, Boston, MA, 1995), pp. 75–118.
[31]T.-C. Jagau, "Theory of electronic resonances: Fundamental aspects and recent advances," Chem. Commun. **58**, 5205–5224 (2022).
[32]B. Mennucci, "11 - multiscale strategies for describing environment effects: From solvents to biomatrices," in *Green Chemistry and Computational Chemistry, Advances in Geen and Sustainable Chemistry*, edited by L. Mammino (Elsevier, 2022), pp. 263–279.
[33]G. Lamoureux, A. D. MacKerell, and B. Roux, "A simple polarizable model of water based on classical drude oscillators," J. Chem. Phys. **119**, 5185–5197 (2003).
[34]E. Boulanger and W. Thiel, "Solvent boundary potentials for hybrid QM/MM computations using classical Drude oscillators: A fully polarizable model," J. Chem. Theory Comput. **8**, 4527–4538 (2012).
[35]S. W. Rick, S. J. Stuart, and B. J. Berne, "Dynamical fluctuating charge force fields: Application to liquid water," J. Chem. Phys. **101**, 6141–6156 (1994).
[36]F. Lipparini and V. Barone, "Polarizable force fields and polarizable continuum model: A fluctuating charges/PCM approach. 1. Theory and implementation," J. Chem. Theory Comput. **7**, 3711–3724 (2011).
[37]M. A. Thompson and G. K. Schenter, "Excited states of the bacteriochlorophyll *b* dimer of *Rhodopseudomonas viridis*: A QM/MM study of the photosynthetic reaction center that includes MM polarization," J. Phys. Chem. **99**, 6374–6386 (1995).
[38]D. Loco, E. Polack, S. Caprasecca, L. Lagardère, F. Lipparini, J.-P. Piquemal, and B. Mennucci, "A QM/MM approach using the amoeba polarizable embedding: From ground state energies to electronic excitations," J. Chem. Theory Comput. **12**, 3654–3661 (2016).
[39]M. Jorge, J. R. Gomes, and A. W. Milne, "Self-consistent electrostatic embedding for liquid phase polarization," J. Mol. Liq. **322**, 114550 (2021).
[40]M. Jorge, J. R. Gomes, and M. C. Barrera, "The dipole moment of alcohols in the liquid phase and in solution," J. Mol. Liq. **356**, 119033 (2022).
[41]M. Kiataki, M. do N. Varella, and K. Coutinho, "New approach to instantaneous polarizable electrostatic embedding of the solvent," J. Mol. Liq. **389**, 122861 (2023).
[42]H. M. Senn and W. Thiel, "QM/MM methods for biomolecular systems," Angew. Chem., Int. Ed. **48**, 1198–1229 (2009).
[43]J. Nochebuena, S. Naseem-Khan, and G. A. Cisneros, "Development and application of quantum mechanics/molecular mechanics methods with advanced polarizable potentials," WIREs Comput. Mol. Sci. **11**, e1515 (2021).
[44]J. Tomasi, B. Mennucci, and R. Cammi, "Quantum mechanical continuum solvation models," Chem. Rev. **105**, 2999–3094 (2005).
[45]B. Mennucci, "Polarizable continuum model," WIREs Comput. Mol. Sci. **2**, 386–404 (2012).
[46]M. R. Provorse, T. Peev, C. Xiong, and C. M. Isborn, "Convergence of excitation energies in mixed quantum and classical solvent: Comparison of continuum and point charge models," J. Phys. Chem. B **120**, 12148–12159 (2016).

[47]J. M. Milanese, M. R. Provorse, E. Alameda, and C. M. Isborn, "Convergence of computed aqueous absorption spectra with explicit quantum mechanical solvent," J. Chem. Theory Comput. **13**, 2159–2171 (2017).
[48]Y. Zhang, P. Xie, S. Yang, and K. Han, "Ionization and electron attachment for nucleobases in water," J. Phys. Chem. B **123**, 1237–1247 (2019).
[49]M. Mukherjee, D. Tripathi, M. Brehm, C. Riplinger, and A. K. Dutta, "Efficient EOM-CC-based protocol for the calculation of electron affinity of solvated nucleobases: Uracil as a case study," J. Chem. Theory Comput. **17**, 105–116 (2021).
[50]M. De Vetta, M. F. S. J. Menger, J. J. Nogueira, and L. González, "Solvent effects on electronically excited states: QM/continuum versus QM/explicit models," J. Phys. Chem. B **122**, 2975–2984 (2018).
[51]A. Pérez-Barcia, G. Cárdenas, J. J. Nogueira, and M. Mandado, "Effect of the QM size, basis set, and polarization on QM/MM interaction energy decomposition analysis," J. Chem. Inf. Model. **63**, 882–897 (2023).
[52]K. Coutinho and S. Canuto, "Solvent effects in emission spectroscopy: A Monte Carlo quantum mechanics study of the n ← π^* shift of formaldehyde in water," J. Chem. Phys. **113**, 9132–9139 (2000).
[53]C. M. Breneman and K. B. Wiberg, "Determining atom-centered monopoles from molecular electrostatic potentials. The need for high sampling density in formamide conformational analysis," J. Comput. Chem. **11**, 361–373 (1990).
[54]H. M. Cezar, S. Canuto, and K. Coutinho, "Solvent effect on the *syn/anti* conformational stability: A comparison between conformational bias Monte Carlo and molecular dynamics methods," Int. J. Quantum Chem. **119**, e25688 (2019).
[55]A. D. Becke, "Density-functional thermochemistry. III. The role of exact exchange," J. Chem. Phys. **98**, 5648–5652 (1993).
[56]C. Lee, W. Yang, and R. G. Parr, "Development of the Colle–Salvetti correlation-energy formula into a functional of the electron density," Phys. Rev. B **37**, 785–789 (1988).
[57]M. J. Frisch, G. W. Trucks, H. B. Schlegel, G. E. Scuseria, M. A. Robb, J. R. Cheeseman, G. Scalmani, V. Barone, B. Mennucci, and G. A. Petersson *et al.*, *Gaussian 09, Revision D.01*, Gaussian, Inc., Wallingford, CT, 2009.
[58]G. Scalmani and M. J. Frisch, "Continuous surface charge polarizable continuum models of solvation. I.General formalism," J. Chem. Phys. **132**, 114110 (2010).
[59]V. Manzoni, M. L. Lyra, R. M. Gester, K. Coutinho, and S. Canuto, "Study of the optical and magnetic properties of pyrimidine in water combining PCM and QM/MM methodologies," Phys. Chem. Chem. Phys. **12**, 14023–14033 (2010).
[60]C. C. Vequi-Suplicy, K. Coutinho, and M. T. Lamy, "Electric dipole moments of the fluorescent probes Prodan and Laurdan: Experimental and theoretical evaluations," Biophys. Rev. **6**, 63–74 (2014).
[61]L. S. Dodda, I. Cabeza de Vaca, J. Tirado-Rives, and W. L. Jorgensen, "LigParGen web server: An automatic OPLS-AA parameter generator for organic ligands," Nucleic Acids Res. **45**, W331–W336 (2017).
[62]H. J. C. Berendsen, J. R. Grigera, and T. P. Straatsma, "The missing term in effective pair potentials," J. Phys. Chem. **91**, 6269–6271 (1987).
[63]T. Yanai, D. P. Tew, and N. C. Handy, "A new hybrid exchange–correlation functional using the Coulomb-attenuating method (CAM-B3LYP)," Chem. Phys. Lett. **393**, 51–57 (2004).
[64]Y. Zhao and D. G. Truhlar, "The M06 suite of density functionals for main group thermochemistry, thermochemical kinetics, noncovalent interactions, excited states, and transition elements: Two new functionals and systematic testing of four M06-class functionals and 12 other functionals," Theor. Chem. Acc. **120**, 215–241 (2008).
[65]J.-D. Chai and M. Head-Gordon, "Systematic optimization of long-range corrected hybrid density functionals," J. Chem. Phys. **128**, 084106 (2008).
[66]J.-D. Chai and M. Head-Gordon, "Long-range corrected hybrid density functionals with damped atom–atom dispersion corrections," Phys. Chem. Chem. Phys. **10**, 6615–6620 (2008).
[67]A. Lange and J. M. Herbert, "Simple methods to reduce charge-transfer contamination in time-dependent density-functional calculations of clusters and liquids," J. Chem. Theory Comput. **3**, 1680–1690 (2007).
[68]C. M. Isborn, B. D. Mar, B. F. E. Curchod, I. Tavernelli, and T. J. Martínez, "The charge transfer problem in density functional theory calculations of aqueously solvated molecules," J. Phys. Chem. B **117**, 12189–12201 (2013).
[69]D. J. Cole and N. D. M. Hine, "Applications of large-scale density functional theory in biology," J. Phys.: Condens. Matter **28**, 393001 (2016).
[70]G. Lever, D. J. Cole, N. D. M. Hine, P. D. Haynes, and M. C. Payne, "Electrostatic considerations affecting the calculated HOMO–LUMO gap in protein molecules," J. Phys.: Condens. Matter **25**, 152101 (2013).
[71]M. R. Provorse Long and C. M. Isborn, "Combining explicit quantum solvent with a polarizable continuum model," J. Phys. Chem. B **121**, 10105–10117 (2017).